AGU PUBLICATIONS

Geochemistry, Geophysics, Geosystems

RESEARCH ARTICLE
10.1002/2015GC006143

Variation of ocean sediment thickness with crustal age

Peter Olson[1], Evan Reynolds[1], Linda Hinnov[1], and Arghya Goswami[1,2]

[1]Department of Earth and Planetary Sciences, Johns Hopkins University, Baltimore, Maryland, USA, [2]Now at Department of Natural Sciences, Northwest Missouri State University, Maryville, Missouri, USA

Key Points:
- Ocean basin sediment thicknesses are fit by cubic polynomials in crustal age
- Present-day accumulation rates match 0–65 Ma global ocean sediment thickness
- Sediment thicknesses on older ocean crust reflect continent collisions and rifting

Correspondence to:
P. Olson,
olson@jhu.edu

Citation:
Olson, P., E. Reynolds, L. Hinnov, and A. Goswami (2016), Variation of ocean sediment thickness with crustal age, *Geochem. Geophys. Geosyst.*, *17*, 1349–1369, doi:10.1002/2015GC006143.

Received 14 OCT 2015
Accepted 12 MAR 2016
Accepted article online 18 MAR 2016
Published online 17 APR 2016

Abstract Global ocean sediment thickness and present-day ocean sediment accumulation rates are analyzed with respect to the age of the underlying ocean crust. Trends in average sediment thickness and present-day accumulation rate are well fit by cubic polynomials in crustal age for the global ocean and for individual ocean basins. Sediment thickness and accumulation rates are larger in the North and South Atlantic and Indian Oceans compared to the Pacific Ocean, primarily because the anomalous sediment accumulations that followed continental rifting and collision in the Atlantic and Indian Ocean basins are missing in the Pacific Ocean. Modern ocean sediment accumulation rates, extrapolated into the past assuming steady state conditions, account within uncertainties for the global average sediment thickness on 0–65 Ma (Cenozoic age) ocean crust, while the profile of anomalously thick sediments on older (Mesozoic age) ocean crust is well fit by adding localized, diffusive sediment transport from a steady state source referenced to the adjacent continental margin. Apart from a distinct 0–5 Ma (Quaternary age) sediment pulse, deviations in average sediment thickness from this simple model are generally small and are uncorrelated across ocean basins.

1. Introduction

The accumulation of sediments on the ocean floor represents the primary mass transfer from the continental crust to the oceanic crust. It is generally assumed that, over 100×10^6 year time scales, the mass transfer from continental to oceanic crust in the form of pelagic and terrigenous sediments nearly compensates the mass transfer of sediments back onto the continental crust through accretionary processes at convergent margins [*Clift et al*., 2009; *Howell and Murray*, 1986; *Wilkinson and Walker*, 1988] tending to stabilize the total mass of the continental crust as well as the continental freeboard, the mean elevation of the continents with respect to sea level [*Schubert and Reymer*, 1985].

Ocean sediment accumulation has fundamental implications for Earth's long-term climate. The stability of Earth's climate on time scales longer than millions of years is thought to be maintained through a balance between the rate of emission of carbon from Earth's interior by volcanic and metamorphic processes and the rate of carbon removal from the surface environment by carbonate deposition following the weathering of silicate rocks and burial of organic carbon in sediments [*Walker et al*., 1981; *Berner and Kothavala*, 2001; *Berner*, 2004; *Ridgwell and Zeebe*, 2005; *Goudie and Viles*, 2012; *Royer*, 2014]. It has been shown that, under a wide range of conditions, chemical weathering rates on land increase roughly in proportion to the rates of denudation of the continental crust [*West et al*., 2005; *Gabet and Mudd*, 2009], so that the accumulation rate of marine silicate-bearing sediments and marine carbonate sediments whose calcium and magnesium were derived from chemical weathering reflects the overall weathering rate of continental crust. The rate of sediment accumulation in the ocean therefore represents a global indicator of the strength of the "sink" portion of the long-term carbon cycle, and ocean sediment thicknesses provide a time-integrated measure of this sink. In addition to their direct role in the slow carbon cycle, ocean sediments alter the bathymetry of ocean basins by shoaling the water column and reducing bottom roughness, affecting ocean temperature, chemistry, and circulation. Accordingly, there are ample reasons to quantify ocean sediment accumulation patterns and rates, for application to modern environments as well as environments in the geologic past.

There is a long-simmering debate concerning the apparent variations in global sediment accumulation rates versus age, centered on whether these variations mostly reflect tectonic events, responses to changes in the global mean climate, biosphere evolution, or biases related to selective measurement and preservation. Global ocean sedimentation rates inferred from compilations of marine sediment cores [*Southam and Hay*,

1977] show substantial variability through the Cenozoic and Late Mesozoic, including a twofold increase during 0–5 Ma [*Zhang et al*., 2001; *Molnar*, 2004] and a less intense but longer-lived increase in the mid-Cretaceous around 80–90 Ma [*Hay et al*., 1988; *Wold and Hay*, 1990], suggesting a global-scale increase in erosion and deposition rates in the Quaternary and also during the mid-Cretaceous warm period. However, the significance of these variations has been questioned on the grounds that observational biases toward areas with rapid sediment accumulation combined with the statistical decrease in preservation with increasing age leads to spurious inferences about accumulation rate with increasing sediment age [*Willenbring and von Blanckenburg*, 2010; *Willenbring et al*., 2013].

Here we use global distributions of sediment thickness and sediment accumulation rates in the modern ocean in conjunction with high-resolution crustal age distributions to quantify the patterns of sediment thickness and accumulation rate on ocean crust back to 150 Ma. First we parameterize the average thickness of marine sediments and their present-day rate of accumulation in terms of the age of the underlying ocean crust, globally as well as for individual ocean basins. We then demonstrate that that the present-day accumulation rate applied backward in time accounts, within the scatter of the data, for the increase in average ocean sediment thickness on ocean crust back to 65 Ma. In addition, we show that the accumulation rates versus sediment age calculated by *Hay et al*. [1988] from DSDP records, including a prominent 0–5 Ma spike in accumulation rate, account for the average sediment thickness on ocean crust back to 75 Ma.

On older ocean crust, where sediment thickness increases through accumulation of terrigenous material derived from nearby continents, we show that prominent spikes in sediment thicknesses in the North and South Atlantic are synchronous with rifting events in those ocean basins, and that a comparable sediment spike in the Indian Ocean is attributable to the India-Asia continent collision. These sediment spikes are parameterized as diffusively controlled correction terms referenced to their adjacent continental margins. Last, searches for sediment accumulation anomalies fail to show coherence among the major ocean basins, supporting our conclusion that the primary triggers for deviations from steady state sediment accumulation in the world ocean are plate tectonic, rather than global climate or biosphere changes.

2. Previous Work

Most previous studies of the global ocean sediment budget have been concerned with calculating the mass of preserved ocean sediment versus sediment age using data obtained from oceanic sediment cores, and applying statistical models of sediment deposition, recycling, and preservation in order to estimate the actual mass of sediment deposited versus time in the past (see *Veizer and Mackenzie* [2014] for a review of the methods involved). Although it is a fundamental property of the Earth system, accurate estimates of the ocean sediment accumulation in the deep past are problematic, partly because the extreme lateral heterogeneity in ocean sediments makes it difficult to precisely determine the preserved (i.e., present-day) mass versus sediment age relation from a relatively small number of drill sites, and partly because subduction and accretion processes have selectively removed ocean sediments, particularly older-aged sediments, making the conversion from preserved mass to accumulated mass increasingly uncertain going backward in time. In spite of these difficulties and limitations, there are several widely used global compilations of the preserved mass-age relation for ocean sediments [*Lisitzin*, 1996; *Davies and Worsley*, 1981; *Hay et al*., 1988; *Wold and Hay*, 1990] that have been used for these types of extrapolations.

We have found that the compilation by *Hay et al*. [1988] is particularly useful in the context of our study. *Hay et al*. [1988] give tables of total sediments in units of column density (mass per area of ocean crust), binned according to sediment age. Their approach allows for estimation of global sediment accumulation rate as a function of age, partially circumventing the problems associated with selective preservation. Our approach nevertheless differs from *Hay et al*. [1988] in that we focus on variations in sediment thickness and accumulation rate parameterized by age of the underlying ocean crust, rather than the age of the sediments themselves. This approach makes available a far larger sample size—on the order 10^7 individual sediment thicknesses—allowing us to average out much of the spatial heterogeneity that characterizes ocean sedimentation, while simultaneously minimizing biases related to recycling and selective preservation. It has the further advantage that paleooceanographic reconstructions parameterize many ocean properties in terms of the ocean crustal age.

The main limitations of our approach, with regard to reconstructing the history of ocean sediment accumulation, stem from the fact that the age we use is that of the underlying basaltic crust, not the sediments that

Table 1. Statistics of Global Ocean Sediments Used in This Study[a]

Basin	Total Sediment Volume[b] (km^3)	Total Present Day Sed. Rate (km^3/yr)	Total Sediment Mass[b] (kg)	Total Basin Area (km^2)	Average Sed. Rate (m/Ma)
Global	1.516×10^8	1.805	2.977×10^{20}	3.627×10^8	4.976
Indian	4.301×10^7	0.5048	8.979×10^{19}	7.062×10^7	7.149
N. Atlantic	2.487×10^7	0.4762	4.274×10^{19}	4.165×10^7	11.43
N. Pacific	1.553×10^7	0.09621	2.671×10^{19}	7.715×10^7	1.247
S. Atlantic[c]	2.293×10^7	0.3933	4.782×10^{19}	4.029×10^7	9.762
S. Pacific	1.271×10^7	0.3079	2.165×10^{19}	8.500×10^7	3.623

[a]Sediment mass is calculated using sediment thicknesses from Figure 1 and the Hamilton [1976] column average density versus depth curve in Figure 5.
[b]Volume and mass totals are from 0 to 150 Ma.
[c]S. Atlantic totals are from 0 to 140 Ma.

overlie it. It is an obvious fact that sediment thickness depends on many factors, crustal age being just one of these. However, we demonstrate in this paper that ocean crustal age is a robust variable for parameterizing average sediment thicknesses, not only for the global ocean but also for individual ocean basins, and that for our purposes it is superior to some other ocean variables, in particular, the depth of the water column. Furthermore, we show that the present-day sediment accumulation rate can also be parameterized in terms of the crustal age, which allows us to model sediment thickness in terms of its accumulation rate in the modern ocean.

Other, less bothersome disadvantages of our approach stem from converting thickness to column-averaged density, requiring the application of a sediment compaction model, which is nonunique and introduces additional uncertainties, as described above. In this study, we mostly report our results in terms of the primary data, sediment thickness, using column-averaged densities derived from standard compaction models only for calculating sediment mass and for comparison with previous sediment accumulation models. We also compare our parameterized sediment thickness profiles with previous crustal age parameterizations [*Spinelli et al*., 2004; *Müller et al*., 2008b; *Conrad*, 2013] as well as the sediment thickness parameterized in terms of sediment age obtained from the *Hay et al*. [1988] compilation.

3. Ocean Sediment Data

In this study, we use well-documented, global data sets for ocean depth, ocean crustal age, ocean sediment thickness, and ocean sediment accumulation rate, projected onto identical uniform 0.1 × 0.1 latitude-longitude grids. For ocean depth, we use ETOPO1 seafloor depths [*Amante and Eakins*, 2009]. For ocean crust ages, we use the present-day reconstruction by *Müller et al*. [2008a,b]. For ocean sediment thicknesses, we use the global data set compiled by *Divins* [2003] as augmented by *Whittaker et al*. [2013], and for present-day ocean sediment accumulation rates, we use the compilation by *Archer* [1996b]. The *Archer* [1996b] compilation is based on sediment core data from *Cwienk* [1986] together with data later published by *Catubig et al*. [1998]. These combined data were first normalized to non-$CaCO_3$ material mass accumulation rate, then weight averaged with respect to distance and depth to account for higher terrigenous sediment near continents, water column opal redissolution, and carbonate-opal burial interactions. The resulting non-$CaCO_3$ accumulation rate gridded map [*Archer*, 1996b, Figure 3a] was combined with that of dry weight percent $CaCO_3$ in surface sediments from *Archer* [1996a] to produce a total sediment accumulation rate map [*Archer*, 1996b, Figure 3b], which is available at David Archer's website as Gridded sediment accumulation rate, coretop. An additional useful resource is the global compilation of present-day ocean sediment lithology by *Dutkiewicz et al*. [2015].

In comparing these data sets, we find that most of the uncertainty originates in the sediment thickness and sediment accumulation rates, by virtue of their extreme spatial variability. In spite of this spatial variability, however, reproducibly smooth trends emerge when these data are expressed in terms of crustal age averages, and these averages provide estimates of total sediment volumes and total accumulation rates (and to a lesser extent, sediment masses) that are generally consistent with previous studies. In Table 1, for example, the estimate of the total sediment volume on ocean crust between 0 and 150 Ma age based on the data sets above is 1.516×10^8 km^3, comparable to 1.55×10^8 km^3 obtained by *Southam and Hay* [1977]

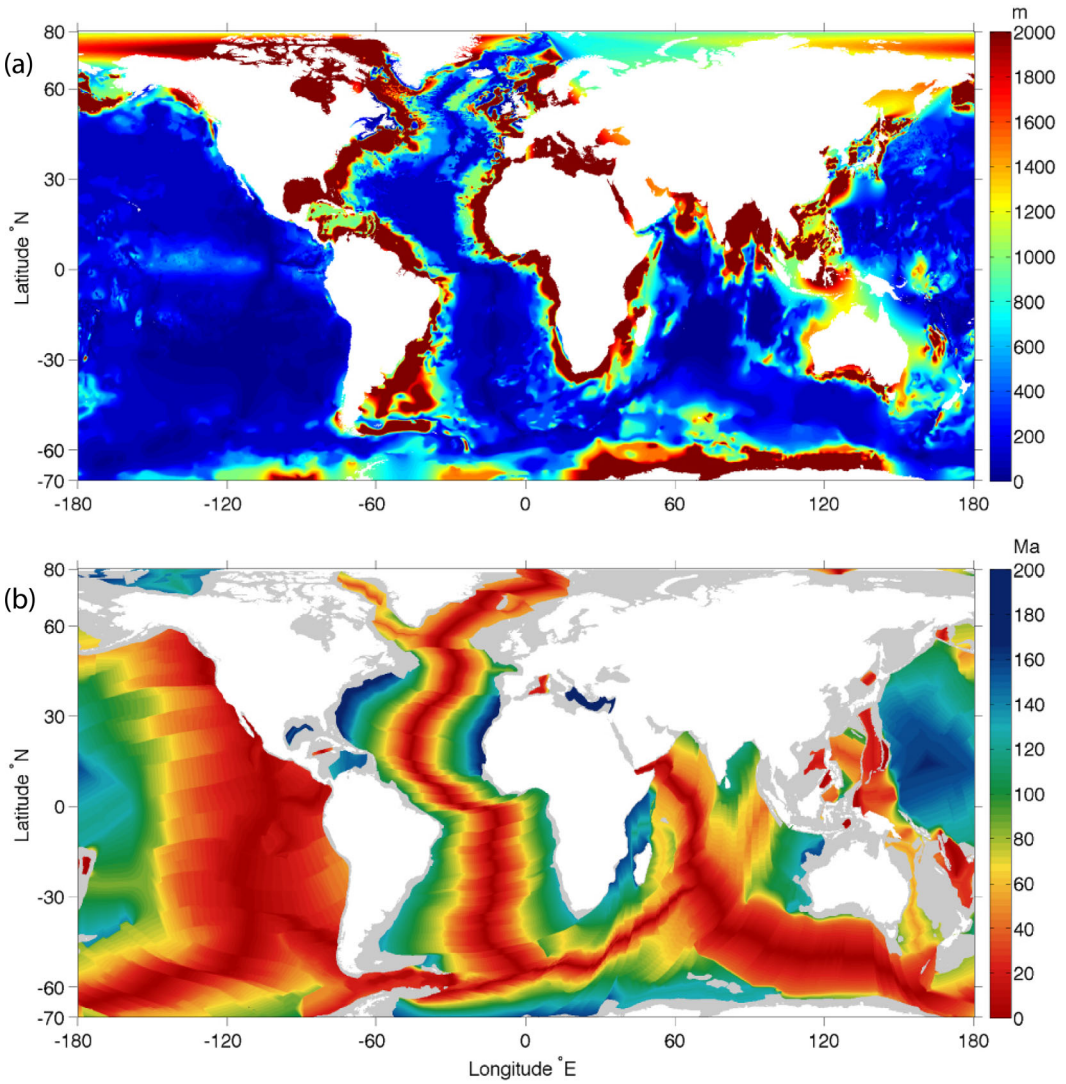

Figure 1. (a) Global ocean sediment thickness saturated at 2000 m. From *Divins* [2003] and *Whittaker et al*. [2013]. (b) Age of the ocean crust used in this study, from *Müller et al*. [2008b].

and 1.42×10^8 km^3 obtained by *Howell and Murray* [1986], discrepancies of just 2% and 6%, respectively. These contrast with the compilation by *Lisitzin* [1996] that yielded just 1.22×10^8 km^3, a discrepancy which is probably attributable to systematic differences in areas of the ocean crust sampled by *Lisitzin* [1996] versus the other three studies.

Larger discrepancies result when sediment volumes are converted to sediment mass. For example, from Table 1, our total pelagic sediment mass for 0–150 Ma crustal age is 2.98×10^{20} kg, versus 2.61×10^{20} kg estimated by *Hay et al*. [1988] for the mass of sediments with the same age range, an 11% discrepancy. A portion of this discrepancy may due to the difference between crustal age used in our compilation and sediment age used by *Hay et al*. [1988], but additional discrepancy comes from uncertainties in sediment density, which is needed to convert volume to mass. Accordingly, in this study, we use sediment thicknesses or volumes, rather than sediment masses or column densities wherever possible, thereby avoiding the conversion from volume to mass.

4. Global Maps

Figure 1a shows the global distribution of ocean sediment thickness from the compilation by *Divins* [2003] and extended by *Whittaker et al*. [2013]. The thickness scale has been saturated at 2000 m in order to

highlight the variations within the interiors of the ocean basins. Thick sediment accumulations dominate the continental margins of the Atlantic and Indian Oceans that are largely missing from the Pacific Ocean. In contrast, the sediments are much thinner within the interior of all of the ocean basins. Statistics of the sediment distribution drawn from this map are given in Table 1. Figure 1b shows the global distribution of ages of ocean crust from the compilation of *Müller et al*. [2008b]. Crustal ages range from 0 Ma (present day) at mid-oceanic spreading centers to slightly more than 180 Ma in the northwestern Pacific, eastern Mediterranean, and along the margins of the North Atlantic. Comparing Figures 1a and 1b, a general correlation of sediment thickness with crustal age is evident.

In addition to the age of the underlying crust, there are multiple factors that contribute to the heterogeneity in ocean sediment thickness. These include (1) the tectonic history of the ocean basin, (2) structural heterogeneity of the basement, (3) spatial heterogeneity of terrigenous sediment sources, (4) spatial heterogeneity of the oceanographic processes that deliver sediments, and (5) temporal evolution of the global climate, erosion, and weathering rates, and the abundance of pelagic calcifiers. Some of these sources of heterogeneity can be reduced by averaging the sediment thicknesses globally, or by averaging over separate ocean basins. Global or basin-scale averaging is particularly useful in reducing heterogeneity due to item (2), and also to some extent, the regional-scale heterogeneities related to items (1), (3), and (4). In addition, by parameterizing sediment thickness with respect to underlying crustal age, we collapse much of the remaining heterogeneity, particularly as applies to global-scale causes represented by items (1), (4), and (5).

A simple illustration of the systematic trends in ocean sediment thickness that also serves to highlight departures from those trends is to plot the time average rate of ocean sediment accumulation, i.e., the ratio of sediment thickness in Figure 1a to crustal age in Figure 1b. The resulting map is shown in Figure 2a. This map shows time averaged sediment accumulation rates on oceanic crust, this is, only those locations where ocean crust ages are available. Data on the continental shelves and rises without ocean crust ages have been omitted and are replaced with zero values on this map. Very high time average sediment accumulation rates—35 m Ma^{-1} or above—are largely restricted to mid-ocean ridge crest regions, continental margins, and a few anomalously shallow oceanic areas. Over most of the ocean basins, the time average accumulation rate is 10 m Ma^{-1} or less, and as Table 1 indicates, the global average rate is about 5 m Ma^{-1}.

Figure 2b shows the present-day ocean sediment accumulation rates from the compilation by *Archer* [1996b], plotted using the same color scale as Figure 2a. If the ocean basins were static, that is, if seafloor spreading was negligible over the period of time these sediments accumulated, and if the present-day accumulation rates applied equally in the past, then the maps in Figures 2a and 2b would match. Although these maps are broadly similar in their overall patterns, there are nevertheless significant differences, especially near passive and collision-type continental margins, where the long-term average accumulation rates are higher than present-day. In the following sections, we provide evidence that ocean sediment accumulation rates spiked following continental rifting and collision events to produce the differences in the maps in Figures 2a and 2b near the continental margins, and we argue that the primary controls on the variability of ocean sediment accumulation are plate tectonic, rather than climate change or other causes.

5. Global Profiles

Figure 3 shows the global profile of ocean sediment thickness versus crustal age from 0 to 120 Ma, extracted from the data in Figures 1a and 1b. In compiling this profile, we sample the sediment thickness and crustal age in $0.1^\circ \times 0.1^\circ$ polygons, then bin the data in 1 Ma age bins. Polygon area weighting is applied in computing the means, percentiles, and standard deviations within each 1 Ma bin. The blue dots in Figure 3 represent bin means, the red dots represent the 25th and 75th percentiles in each bin, and the grey and red error bars represent, respectively, one standard deviation of the data in each bin and the standard deviation of the bin mean.

The global mean sediment thickness increases with crustal age almost monotonically from 0 Ma to approximately 83 Ma. On older crust, the rate of increase in sediment thickness with crustal age is generally faster than on younger age crust and it is also more heterogeneous, as reflected in increased standard deviation of the data with crustal age. In addition, the heterogeneity is highly asymmetric: in each age bin there are far more polygons with thin sediments than with thick sediments. This asymmetry is reflected in the Figure 3 insert, which shows that the frequency distribution for the global ocean is highly skewed toward thin

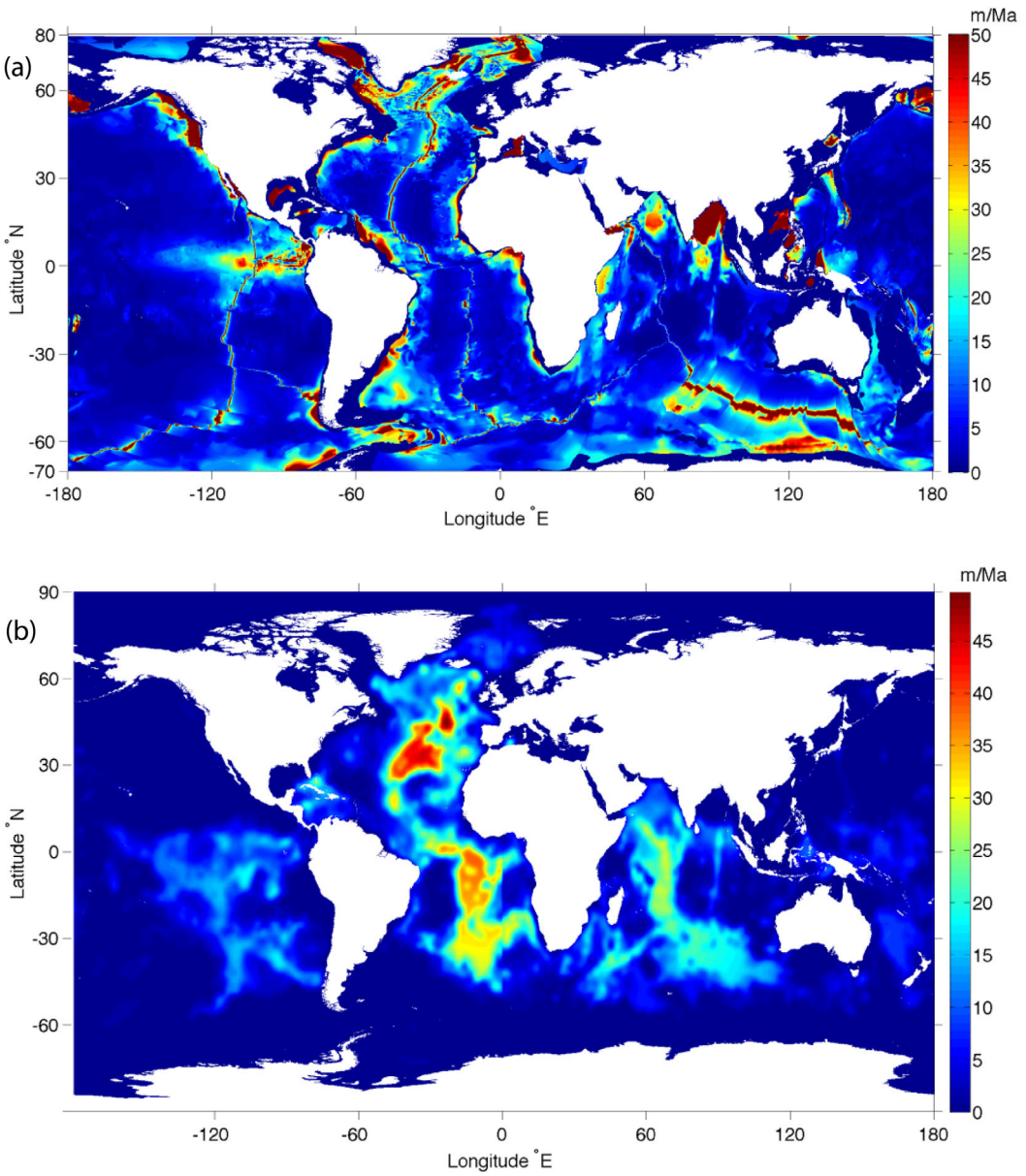

Figure 2. (a) Global time average ocean sediment accumulation rate, the ratio of Figures 1a and 1b. (b) Present-day global ocean sediment accumulation rate, from *Archer* [1996b].

sediments, and decreases superexponentially with increasing sediment thickness. This extreme skewness explains why the 75th percentile thickness falls below the mean of the data for crustal ages greater than about 90 Ma, whereas the 25th percentile thickness remains small at all ages.

Despite the skewness and the greater variability at older ages, the trend of the bin means is well described in terms of low-order polynomials in crustal age. Figure 3 also shows regression fits to linear, quadratic, and cubic polynomials, with the coefficients and RMS errors of each fit given in Table 2. A simple cubic polynomial fits the 0–120 Ma thickness profile remarkably well, particularly for crustal ages less than 83 Ma. The qualitative trends in Figure 3 have been noted in previous compilations of sediment thickness versus crustal age for the global and Atlantic ocean [*Spinelli et al*., 2004; *Müller et al*., 2008a; *Conrad*, 2013]; and separately with linear fits in the Atlantic and Pacific [*Conrad*, 2013]. The size of the RMS residuals in Table 2 shows that a cubic polynomial fit is a far better characterization of the global mean thickness variation, and cubic polynomials also provide far better fits in the Atlantic and Pacific basins. In the next section, we show that this

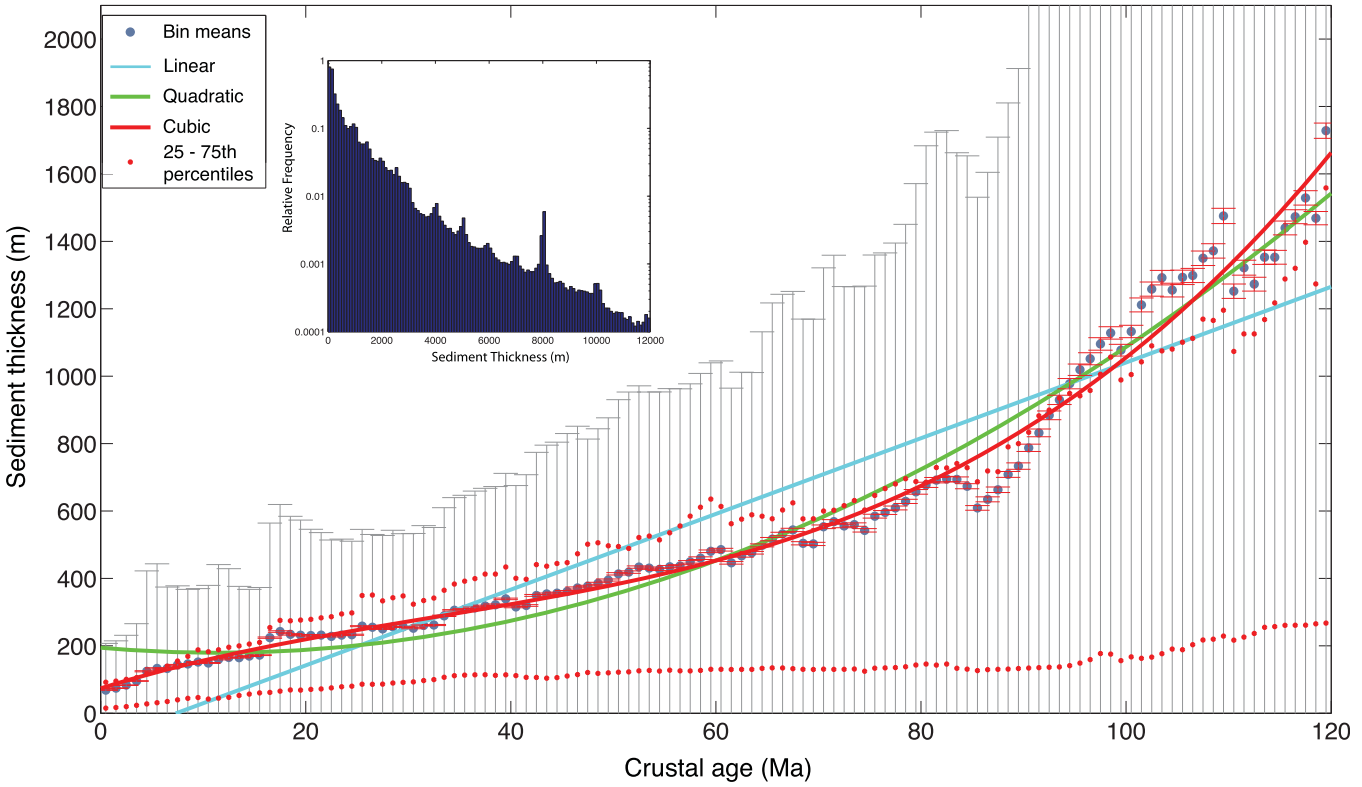

Figure 3. Profile of global ocean sediment thickness versus crustal age. Large dots and gray error bars denote bin means and standard deviations; red error bars denote standard error of the bin mean; small red dots denote 25th and 75th percentiles for each bin. Solid lines are linear, quadratic, and cubic polynomial fits to the bin means. Coefficients of the polynomial fits are given in Table 2. Insert shows the relative frequency distribution for global ocean sediment thickness.

cubic polynomial trend in thickness can be reproduced by superimposing two sources of accumulation: a steady state source equal to the present-day accumulation rate plus a localized correction term that models the time and space-dependent sediment accumulation following continental rifting and collision events.

Figure 4 shows the global profile of the present-day sediment accumulation rate versus crustal age, for ocean crust ranging from 0 to 120 Ma age. This profile was extracted from the maps in Figures 1a and 2b based on the same 0.1° × 0.1° grid used for the global sediment thickness profile. In spite of the large scatter within individual bins, the trend of the bin means is relatively smooth, and with the exception of several isolated bins around 12, 27, 54, and 63 Ma, the bin means of the present-day accumulation rate are well fit by a cubic polynomial in crustal age, with coefficients given in Table 2. The dashed curve labeled DSDP in Figure 4 shows sediment thickness versus sediment age calculated using the mass-sediment age relationship proposed by *Hay et al*. [1988] based on Deep Sea Drilling Project core data. The *Hay et al*. [1988] compilation gives the average sediment mass per area of ocean crust in 5 Ma sediment age bins, starting from the present day. To convert their sediment mass per area to sediment thickness, we have applied the compaction model of *Hamilton* [1976] shown in Figure 5.

Figure 4 shows that the present-day sediment accumulation rate approximates a lower-bound envelope for the *Hay et al*. [1988] profile, with the most significant deviations occurring between 0 and 5 Ma, 38 and 65 Ma, and around 85 Ma, where the *Hay et al*. [1988] profile exceeds the modern accumulation rate profile. It is remarkable that these profiles agree at all, and in particular, that they show overall similar downward trends with increasing age.

The conventional interpretation of downward trend of the present-day profile in Figure 4 is that the accumulation rate of carbonates is higher today on the flanks of the mid-ocean ridges, where the crust is young, compared to older ocean crust [*Archer*, 1996a,b]. Conventional interpretations of the downward trend of the dashed curve in Figure 4 include ocean sediment recycling [*Veizer and Mackenzie*, 2014] and overall decline in the abundance of pelagic calcifiers with increasing age [*Mackenzie and Morse*, 1992; *Ridgwell and*

Table 2. Coefficients of Polynomial Fits to Mean Ocean Sediment Thickness Versus Crustal Age and Modern Ocean Sediment Accumulation Rate Versus Crustal Age: $y=c_0+c_1\tau+c_2\tau^2+c_3\tau^3$[a]

Thickness (m)	Polynomial	c_0	c_1	c_2	c_3	RMS (m)
Global	Linear	-8.246×10^{1}	1.123×10^{1}	0	0	1.431×10^{2}
Global	Quadratic	1.945×10^{2}	-2.618	1.154×10^{-1}	0	7.172×10^{1}
Global	Cubic	7.389×10^{1}	9.443	-1.358×10^{-1}	1.396×10^{-3}	5.539×10^{1}
Indian	Linear	-3.813×10^{2}	2.002×10^{1}	0	0	3.740×10^{2}
Indian	Quadratic	3.537×10^{2}	-1.673×10^{1}	3.062×10^{-1}	0	1.786×10^{2}
Indian	Cubic	-3.399×10^{1}	2.203×10^{1}	-5.013×10^{-1}	4.5×10^{-3}	1.023×10^{2}
N. Atlantic	Linear	-2.038×10^{2}	1.693×10^{1}	0	0	2.383×10^{2}
N. Atlantic	Quadratic	2.955×10^{2}	-1.133×10^{1}	2.666×10^{-1}	0	1.130×10^{2}
N. Atlantic	Cubic	1.548×10^{1}	2.036×10^{1}	-4.808×10^{-1}	4.700×10^{-3}	5.375×10^{1}
N. Pacific	Linear	2.351×10^{2}	-2.944×10^{-1}	0	0	3.588×10^{1}
N. Pacific	Quadratic	2.270×10^{2}	1.327×10^{-1}	-3.502×10^{-3}	0	3.572×10^{1}
N. Pacific	Cubic	1.712×10^{2}	5.953	-1.309×10^{-1}	7.268×10^{-4}	2.810×10^{1}
S. Atlantic	Linear	-3.658×10^{2}	1.620×10^{1}	0	0	3.850×10^{2}
S. Atlantic	Quadratic	3.717×10^{2}	-2.067×10^{1}	3.073×10^{-1}	0	1.988×10^{2}
S. Atlantic	Cubic	-8.261×10^{1}	2.474×10^{1}	-6.389×10^{-1}	5.256×10^{-3}	1.003×10^{2}
S. Pacific	Linear	6.367×10^{1}	1.571	0	0	3.375×10^{1}
S. Pacific	Quadratic	8.762×10^{1}	2.066×10^{-1}	1.113×10^{-2}	0	3.239×10^{1}
S. Pacific	Cubic	2.174×10^{1}	7.267	-1.486×10^{-1}	9.273×10^{-4}	1.798×10^{1}
N+S Atlantic	Linear	-1.656×10^{2}	1.314×10^{1}	0	0	2.068×10^{3}
N+S Atlantic	Quadratic	2.328×10^{2}	-9.406	2.127×10^{-1}	0	9.569×10^{2}
N+S Atlantic	Cubic	6.141	1.624×10^{1}	-3.922×10^{-1}	3.804×10^{-3}	3.735×10^{2}
N+S Pacific	Linear	1.348×10^{2}	8.520×10^{-1}	0	0	3.978×10^{2}
N+S Pacific	Quadratic	1.027×10^{2}	2.539	-1.383×10^{-2}	0	3.694×10^{2}
N+S Pacific	Cubic	5.250×10^{1}	7.775	-1.284×10^{-1}	6.538×10^{-4}	2.987×10^{2}
Rate (m/Ma)	Polynomial	c_0	c_1	c_2	c_3	RMS (m/Ma)
Global	Linear	9.240	-5.895×10^{-2}	0	0	1.110
Global	Quadratic	1.148×10^{1}	-1.709×10^{-1}	9.328×10^{-4}	0	4.804×10^{-1}
Global	Cubic	1.228×10^{1}	-2.515×10^{-1}	2.612×10^{-3}	-9.331×10^{-6}	3.715×10^{-1}
Indian	Linear	1.192×10^{1}	-7.881×10^{-2}	0	0	7.9772×10^{-1}
Indian	Quadratic	1.214×10^{1}	-9.015×10^{-2}	9.448×10^{-5}	0	7.913×10^{-1}
Indian	Cubic	1.222×10^{1}	-9.812×10^{-2}	2.605×10^{-4}	-9.225×10^{-7}	7.907×10^{-1}
N. Atlantic	Linear	2.470×10^{1}	-1.794×10^{-1}	0	0	1.893
N. Atlantic	Quadratic	2.626×10^{1}	-2.673×10^{-1}	8.297×10^{-4}	0	1.332
N. Atlantic	Cubic	2.363×10^{1}	-3.017×10^{-2}	-6.187×10^{-3}	4.413×10^{-5}	9.038×10^{-1}
N. Pacific	Linear	2.888	-2.679×10^{-2}	0	0	9.171×10^{-1}
N. Pacific	Quadratic	4.669	-1.158×10^{-1}	7.419×10^{-4}	0	4.553×10^{-1}
N. Pacific	Cubic	5.482	-1.971×10^{-1}	2.436×10^{-3}	-9.409×10^{-6}	3.360×10^{-1}
S. Atlantic	Linear	1.747×10^{1}	-1.206×10^{-1}	0	0	1.907
S. Atlantic	Quadratic	2.078×10^{1}	-2.861×10^{-1}	1.379×10^{-3}	0	1.203
S. Atlantic	Cubic	1.962×10^{1}	-1.708×10^{-1}	-1.023×10^{-3}	1.335×10^{-5}	1.122
S. Pacific	Linear	5.859	-5.237×10^{-2}	0	0	1.447
S. Pacific	Quadratic	8.654	-1.921×10^{-1}	1.164×10^{-3}	0	7.297×10^{-1}
S. Pacific	Cubic	9.725	-2.992×10^{-1}	3.395×10^{-3}	-1.239×10^{-5}	6.073×10^{-1}

[a]The units of τ (crustal age) are Ma and the units of y are m (thickness) or m/Ma (accumulation rate). All fits are over the range $0 \leq \tau \leq 120$ Ma. RMS misfits are given in the last column.

Zeebe, 2005; *Arvidson et al*., 2014]. According to these interpretations, there is no reason that the two profiles should match, other than coincidence. Apart from coincidence, the only simple explanation for their match is a hypothetical steady state situation, in which the present-day accumulation rate profile also applied to the past. This hypothetical situation ignores the effects from sediment recycling, evolution of calcifiers, and climate change, which are obviously important. However, the fact that the two profiles in Figure 4 show comparable trends and agree in magnitude over significant age ranges indicates that present-day accumulation rates provide a basis for modeling sediment thickness trends throughout the global ocean.

6. Sediment Accumulation Models

Insight into the factors that have controlled ocean sedimentation in the past can be obtained by comparing the predictions of idealized, one-parameter accumulation models with the observed global sediment thickness profile. Assuming that vertical sedimentation through the water column is the only accumulation

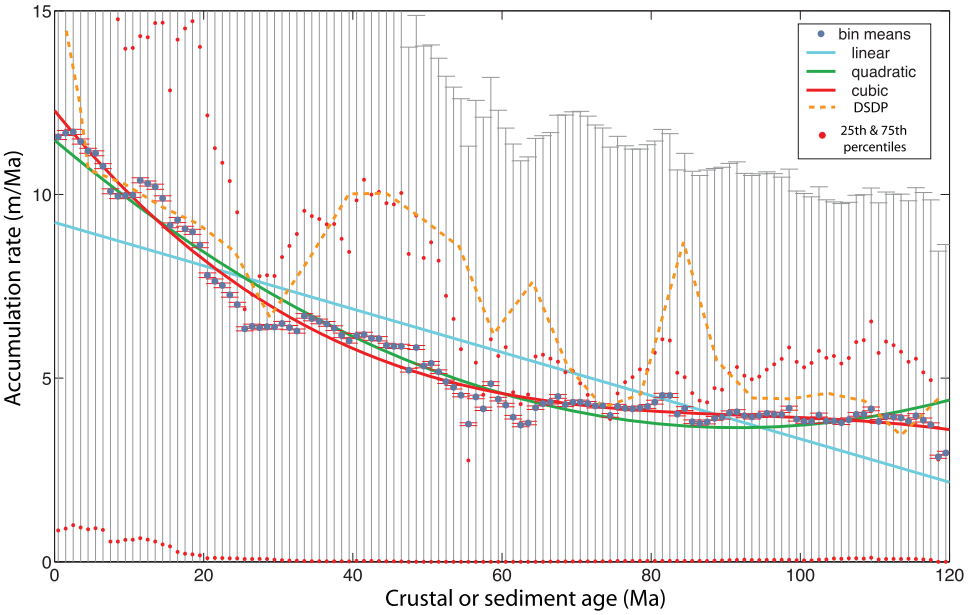

Figure 4. Profiles of global ocean sediment accumulation rate versus age. Large dots and gray error bars indicate bin means and standard deviations of the present-day accumulation rate versus ocean crustal age, with red error bars denoting standard error of the bin mean and small red dots denote 25th and 75th percentiles for each bin. Solid lines are linear, quadratic, and cubic polynomial fits to the bin means. Coefficients of the polynomial fits are given in Table 2. The orange dashed curve shows sediment accumulation rate versus sediment age, derived from the ocean sediment mass-age relationship by *Hay et al.* [1988] from DSDP cores.

mechanism (that is, neglecting postdepositional transfers), the mass balance for a column of ocean sediment can be expressed as

$$\frac{d}{dt}(\bar{\rho}h)=\rho_0 a(\mathbf{x},t) \tag{1}$$

where h is sediment column thickness in m, for example, a is sediment accumulation rate, in m Myr^{-1}, for example, which in general depends on time t and position $\mathbf{x}$, ρ_0 is sediment density at the ocean-sediment interface, and $\bar{\rho}$ is the average density of the sediment column, which depends on column thickness h.

In accord with the results in the previous section, we take as a starting assumption that the accumulation rate a depends only on age τ. Integration of (1) then yields an implicit relationship for h as a function of τ:

$$\bar{\rho}[h]h(\tau)=\rho_0\int_0^{\tau} a(\tau')d\tau' \tag{2}$$

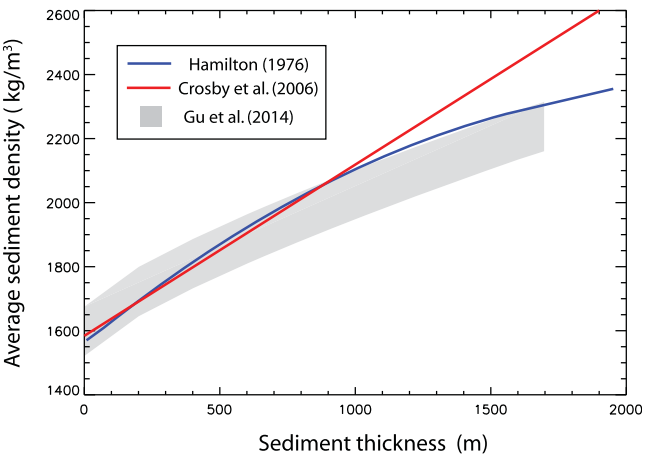

Figure 5. Average sediment density versus sediment thickness. The blue curve is from *Hamilton* [1976] for 60% carbonate, 40% silica + clay. The red curve is from *Crosby et al.* [2006] for 50% carbonate. Gray shading is a fit to DSDP core data by *Gu et al.* [2014] that includes ocean floor density variations.

Two distinct interpretations of τ in (2) are shown in Figure 6. Figure 6a illustrates steady state accumulation, in which the accumulation rate depends only on the local age of the ocean crust. In this case, the age τ in (2) refers to crustal age. Alternatively, Figure 6b illustrates the situation in which the accumulation rate is uniform over the entire ocean but varies with time. In this case, τ in (2) refers to sediment age.

In the steady state accumulation rate model, we use $a(\tau)$ given by the cubic polynomial fit in Table 2 to the present-day accumulation rate profile

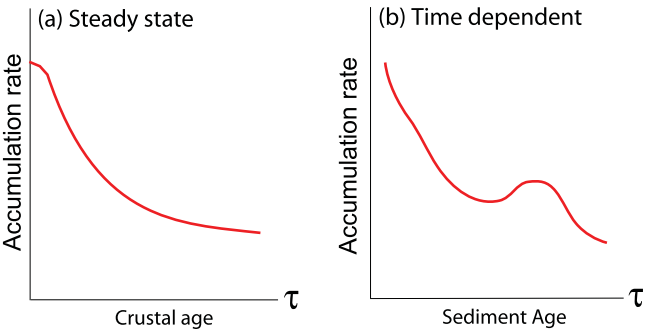

Figure 6. One-parameter ocean sediment accumulation models. (a) Steady state. Accumulation rate is uniform in time but variable in terms of ocean crust age; here τ represents crustal age. (b) Time dependent. Accumulation rate is uniform in space but variable in time; here τ represents sediment age.

shown in Figure 4. In the spatially uniform but time dependent accumulation rate model, we use $a(\tau)$ given by a 1 Ma interpolation of the *Hay et al.* [1988] accumulation rate profile shown in Figure 4. In both cases, we use the column average density $\bar{\rho}(h)$ from *Hamilton* [1976] shown in Figure 5, which is based on an assumed composition of 60% carbonates plus 40% clay. This choice of compaction model differs insignificantly from a model with 50% carbonates used by *Crosby et al.* [2006] for sediment column thicknesses h between 0 and 1100 m. Figure 5 shows that, for thin sediment columns, the *Hamilton* [1976] and *Crosby et al.* [2006] compaction models deviate from a recent model by *Gu et al.* [2014] that factors in a wide range of seafloor sediment densities ρ_0. However, experimentation with different density profiles reveals that our basic results would not change significantly had we used instead average densities from *Gu et al.* [2014].

A comparison of the steady state and time dependent models with the global sediment thickness profile is shown in Figure 7. Here we have extended the global sediment thickness profile to 150 Ma in order to examine longer-term trends. For the steady state model, we adjust its initial sediment thickness to match the observed 0 Ma thickness, but no such adjustment is applied to the time dependent model because the very high accumulation rates in the initial 5 $\times 10^6$ years in the *Hay et al.* [1988] accumulation rate profile have nearly the same effect on the thickness profile as adding a nonzero sediment thickness at zero crustal age.

As seen in Figure 7, both accumulation rate models track the observed average thickness profile out to approximately 40 Ma. Between 40 and 65 Ma, the time dependent model slightly overpredicts the observations, but restores to the observed thickness between 65 and 88 Ma, and interestingly, partially restores to the observed thicknesses on very old ocean crust, beyond 126 Ma. The dotted red curves in Figure 7 denote

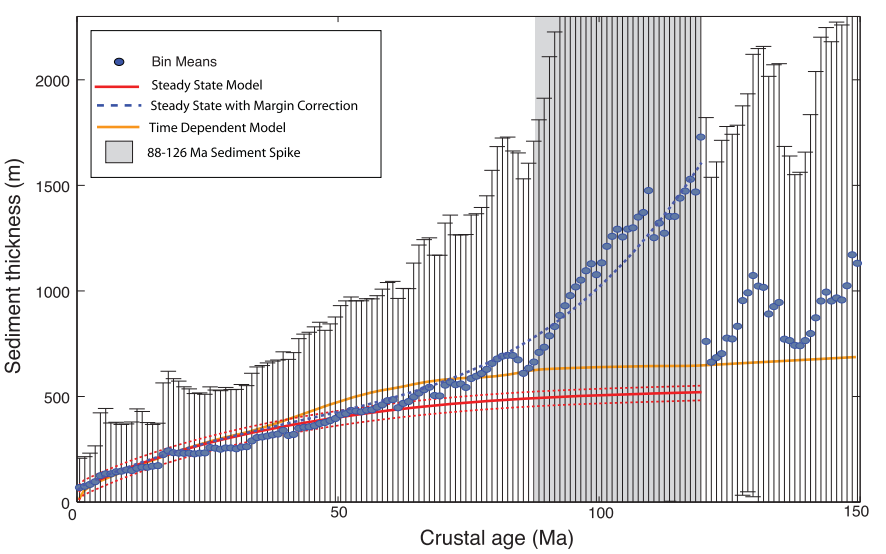

Figure 7. Model fits to global sediment thickness versus age. One million year crustal age bin means and standard deviations are from Figure 1. Cubic fit is from Table 2. Red curve is calculated using the present-day accumulation rate from Table 2 assuming steady state conditions model in Figure 6a. The solid red curve assumes 50 m thickness at zero crustal age and the dotted red curves indicate uncertainties due to sediment compaction. The solid orange curve is calculated using DSDP accumulation rates from *Hay et al.* [1988] in terms of sediment age, assuming time dependent conditions model in Figure 6b. The blue curve applies the correction (4) for anomalous continental margin sedimentation. The highlighted region 88–126 Ma marks age range most affected by anomalous sedimentation.

the range of steady states due to uncertainties in the sediment compaction model and the 0 Ma sediment thickness. Initially, the steady state model closely tracks the observations, but starting around 65 Ma crustal age it too begins to deviate, underpredicting the sediment thickness at older crustal ages by increasing amounts out to 126 Ma.

Given the simplicity of each model, plus the fact that they are based on totally independent data (ancient sediment volumes and ages versus modern sediment volumes), it is remarkable that both yield good results over the entire Cenozoic. However, both models fail to explain the spike in sediment thickness on ocean crust between the ages of 88–126 Ma, and to lesser extents, the secondary spikes on still older crust. The origins of theses spikes are examined in detail in the next section using sediment profiles from the individual ocean basins.

To account the anomalous thickness in the spike in the global profile, we add a correction to each of the one-parameter baseline models that is intended to represent the sum of contributions from localized ocean sediment accumulation adjacent to passively rifted continental margins and seaward of continental collision zones. We model the transport, reworking, and accumulation process at these locations using a one-dimensional diffusion equation [*Smith and Bretherton*, 1972; *Allen and Allen*, 2013]

$$\left(\frac{\partial}{\partial t}-\kappa\frac{\partial^2}{\partial x^2}\right)(\bar{\rho}h')=0 \tag{3}$$

where h' is the anomalous sediment thickness, the difference in sediment thickness in the spike relative to our baseline models, t is time since the anomalous accumulation began, x is distance from the continental margin, and κ is the effective diffusivity that parameterizes the various sediment transport and deposition mechanisms that create the spike. We denote the anomalous sediment mass flux at the continental margin in units of sediment mass delivered per unit time per unit distance along the margin by $F=-\bar{\rho}\kappa(\partial/\partial x)h'(x=0)$. The growth history of the spike is given by the solution to (3) in terms of F:

$$h'=\frac{2F}{\bar{\rho}\kappa}\left(\left(\frac{\kappa t}{\pi}\right)^{1/2}\exp\left(-x^2/4\kappa t\right)-\left(\frac{x}{2}\right)\mathrm{erfc}(x/2\sqrt{\kappa t})\right) \tag{4}$$

where we have assumed that F is constant in time, the column average density $\bar{\rho}$ is uniform in the spike, and the anomalous thickness of the spike h' goes to zero at large x, i.e., far from the continental margin. Distance from the continental margin in (4) can be expressed in terms of crustal ages τ according to

$$x=u(\tau_m-\tau) \tag{5}$$

where $\tau_m=\tau(x=0)$ is the crustal age at the continental margin and u is the average plate spreading rate between crustal ages τ_m and τ.

For the steady state and time dependent baseline models, the sediment anomaly at the peak of the spike is approximately $h'(x=0)=1140$ and 990 m, respectively. We fit (4) and (5) to h' in Figure 7 assuming that $t=126$ Myr and $\tau_m=126$ Ma, corresponding to the age of the oldest crust beneath the sediment spike, and using $u=4\times10^4$ m Ma^{-1} for the average spreading rate of the ocean crust. The fit shown by the blue curve in Figure 7 yields $\kappa=9.5\times10^9$ m^2 Myr^{-1} for both models, with $F/\bar{\rho}=9\times10^6$ m^2 Myr^{-1} for the steady state model and $F/\bar{\rho}=7.9\times10^6$ m^2 Myr^{-1} for the time dependent model. Assuming a mean column of $\bar{\rho}=2300$ kg m^{-3}, the sediment mass fluxes from passively rifted and collisional margins for the two models are $F=2.1\times10^{10}$ kg m^{-1} Myr^{-1} and $F=1.8\times10^{10}$ kg m^{-1} Myr^{-1}, respectively.

According to (4) and (5), the present-day anomalous sediment accumulation rate in the spike is far less than it was in the past. On ocean crust of age τ_m, for example, the present-day rate is predicted to be

$$a'(x=0)=\frac{F/\bar{\rho}}{\sqrt{\pi\kappa\tau_m}} \tag{6}$$

which is only about 4.8 and 4.4 m Myr^{-1} for the steady state and time dependent models, respectively. Comparison with Figure 4 shows that these accumulation rates are comparable to the observed global average accumulation rate on older crust today, implying that the sediment in the spike is mostly old, and the present-day rate of sediment accumulation at these localities is not much greater, on average, than what occurs on similarly aged ocean crust elsewhere.

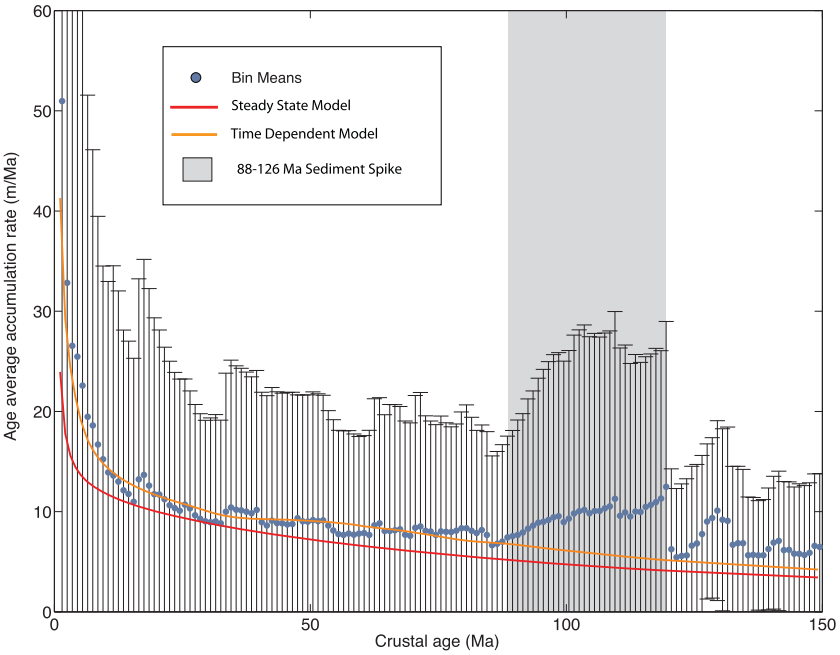

Figure 8. Global ocean average sediment accumulation rate versus crustal age. Model comparisons are described in the text and illustrated in Figure 6.

Additional support for this interpretation is found in Figure 8, which shows the global time average accumulation rate profile versus crustal age for crustal ages 0–150 Ma, the data extracted from the map in Figure 2a. Note the very high accumulation rates on 0–5 Ma age crust. The 25–50 m Ma^{-1} accumulation rates that characterize the youngest part of this record are clearly anomalous: at nearly all other crustal ages, the accumulation rate is 10 m Ma^{-1} or less. Also shown in Figure 8 are the time age average accumulation rates predicted by our steady state and time dependent baseline models. The time dependent, spatially uniform model based on the *Hay et al.* [1988] DSDP compilation is a particularly good match to the observations from 0 to about 88 Ma and also on crust older than 130 Ma. From 88 to 126 Ma, both models fall below the observed accumulation rate, but only by amounts that average 4–4.5 m Ma^{-1}, essentially the same as predicted by our spike correction (6).

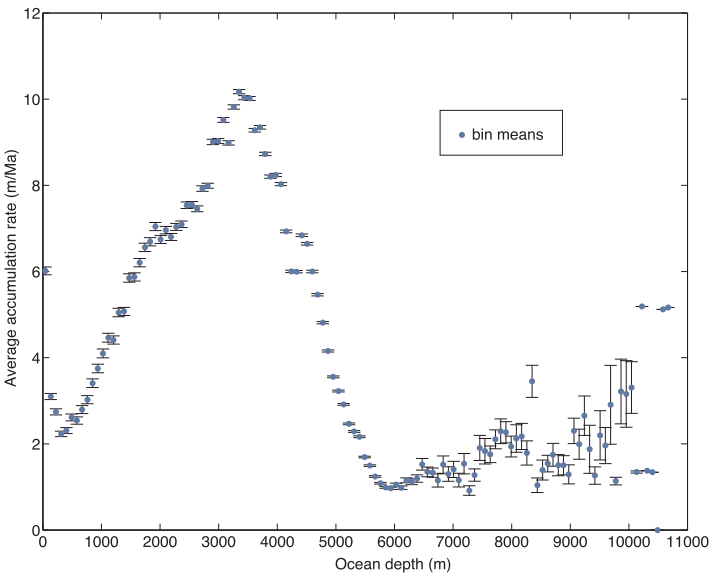

Figure 9. Profile of global ocean average sediment accumulation rate versus ocean depth.

Molnar [2004] interpreted the apparently rapid 0–5 Ma ocean sediment accumulation rates in terms of accelerated weathering and erosion caused by late Cenozoic changes in global hypsometry associated with thickening of continental crust by the India-Asia collision, combined with sea level changes from Pleistocene glaciation. The results in Figure 8 generally support this interpretation, since the primary difference between the time dependent and steady state models, and the main reason that the steady state model deviates from the observations during the Cenozoic is the absence of such

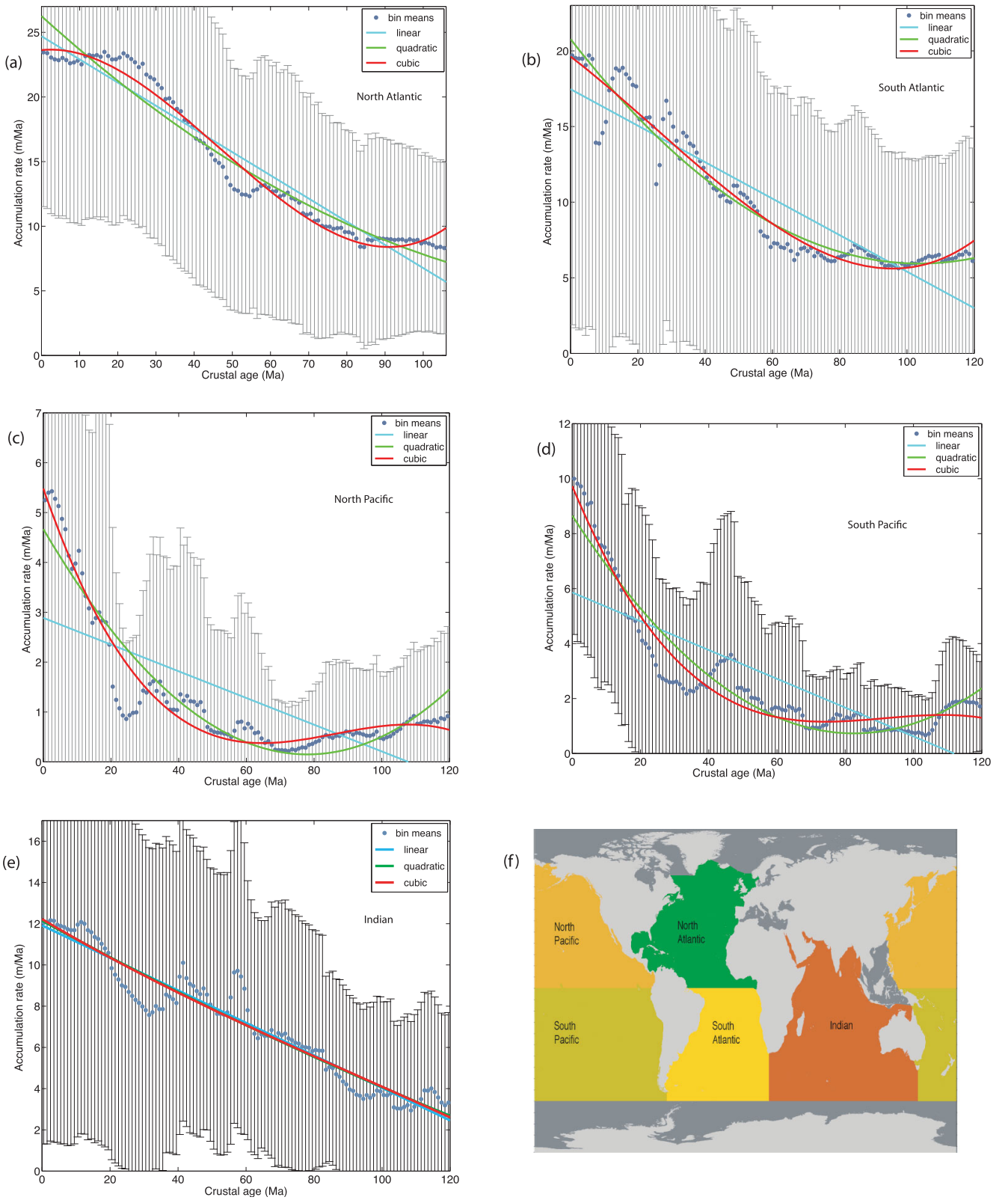

Figure 10. Ocean basin sediment accumulation rate versus crustal age in 1 Ma bins. Dots and error bars indicate bin means and standard deviations. Coefficients of the polynomial fits are given in Table 2. Ocean basins (a) North Atlantic, (b) South Atlantic, (c) North Pacific, (d) South Pacific, (e) Indian, and (f) Reference map showing basin divisions.

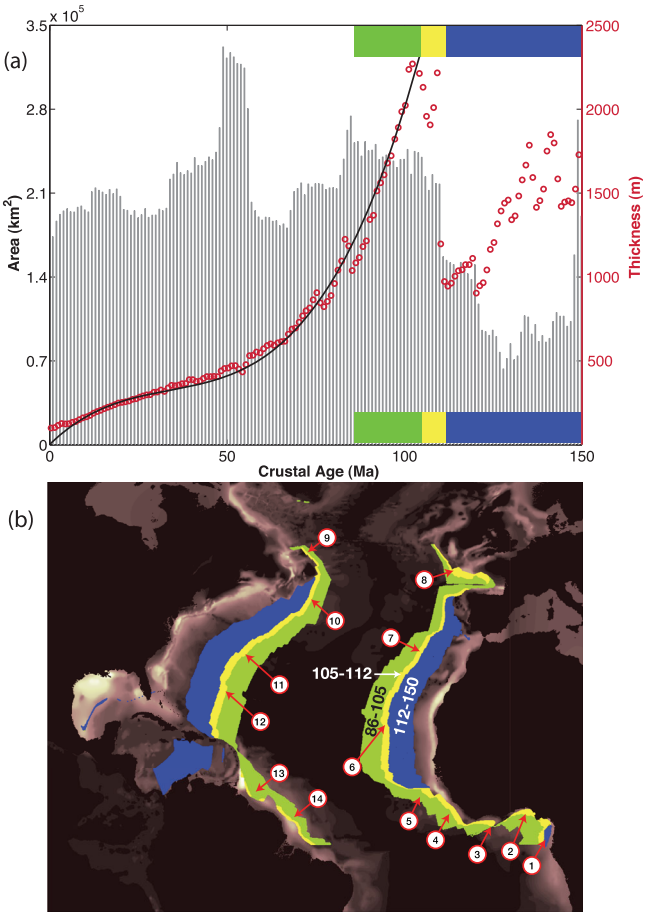

Figure 11. (a) North Atlantic Ocean sediment thickness and area versus crustal age in 1 Ma bins. Dots indicate sediment thickness bin means, bars indicate crustal area in each age bin. Coefficients of the cubic polynomial fit are given in Table 2. Color bars indicate crustal age bands. (b) Map of North Atlantic sediment thickness showing crustal age bands in Ma and basin structures that accommodate the sediment spike: 1 = Northeastern Gulf of Guinea; 2 = Northern Bight of Benin; 3 = Northwestern Guinea Basin (west of Cote d'Ivoire Escarpment); 4 = North-northeastern Sierra Leone Basin; 5 = North of Sierra Leone Rise; 6 = Eastern Cape Verde Basin; 7 = Canary Basin; northward to Iberian Basin; 8 = Bay of Biscay westward along northwestern European Basin; 9 = Southern Labrador Basin; 10 = Newfoundland Basin and central Sohm Abyssal Plain; 11 = Eastern Bermuda Rise; 12 = Southward along Nares Plain to Puerto Rico Trench; 13 = Western Demerara Rise; 14 = Western Ceara Rise.

rapid accumulation at the present day on 0–5 Ma crust.

Finally, we address the issue of whether crustal age is the optimum choice for modeling ocean sediment accumulation and accumulation rate. A seemingly more logical choice would be to parameterize the accumulation rate in terms of the local ocean depth *d*, since water column depth plays a major role in determining sediment lithology, particularly whether carbonate sediments are precipitated or dissolved [*Dutkiewicz et al.*, 2015]. It turns out that ocean depth is not a good parameter choice for this purpose. Figure 9 shows the average present-day accumulation rate versus ocean depth. The accumulation rate initially decreases rapidly with ocean depth to $d = 200$ m, then increases irregularly, peaking around $d = 3300$ m, finally decreasing irregularly to $d = 5500$ m. The explanation for this nonuniform behavior is that very different depositional environments may have similar depths, so that each bin in Figure 9 averages sediment thickness over a heterogeneous set of environments. In contrast, although the variance is high, the more uniformly monotonic behavior in Figures 4 and 8 reflects greater homogeneity of the environments that contribute to each bin. We also examined a parameterization of sediment thickness in terms of latitude, as was done by *Müller et al.* [2008b]. However, for the global ocean, the improvement of the fit was marginal for sediment thickness, and we found no significant improvement for the global ocean accumulation rate.

7. Sediment Profiles in Ocean Basins

Figure 10 shows modern sediment accumulation rates versus crustal age profiles by ocean basin, with the insert map showing the basin subdivisions. These profiles reflect the well-known differences in sedimentation patterns between the Pacific Ocean versus the Indian and Atlantic Oceans, reflecting their differences in plate tectonic history, ridge topography, and river inputs. In particular, the North Atlantic, South Atlantic, and Indian Ocean basins are bounded by extensive passive margins and continent collision zones, providing copious supplies of terrestrial sediments and dissolved constituents, both of which are relatively scarce in the North and South Pacific. Accordingly, the variation of accumulation rate versus crustal age seen in the global profile is more-or-less repeated in the profiles in the North and South Atlantic and Indian Oceans. In contrast, the South Pacific and North Pacific profiles are characterized by much lower rates overall. Low-order polynomial fits to the basin sediment accumulation rate profiles are given in Table 2. As with the

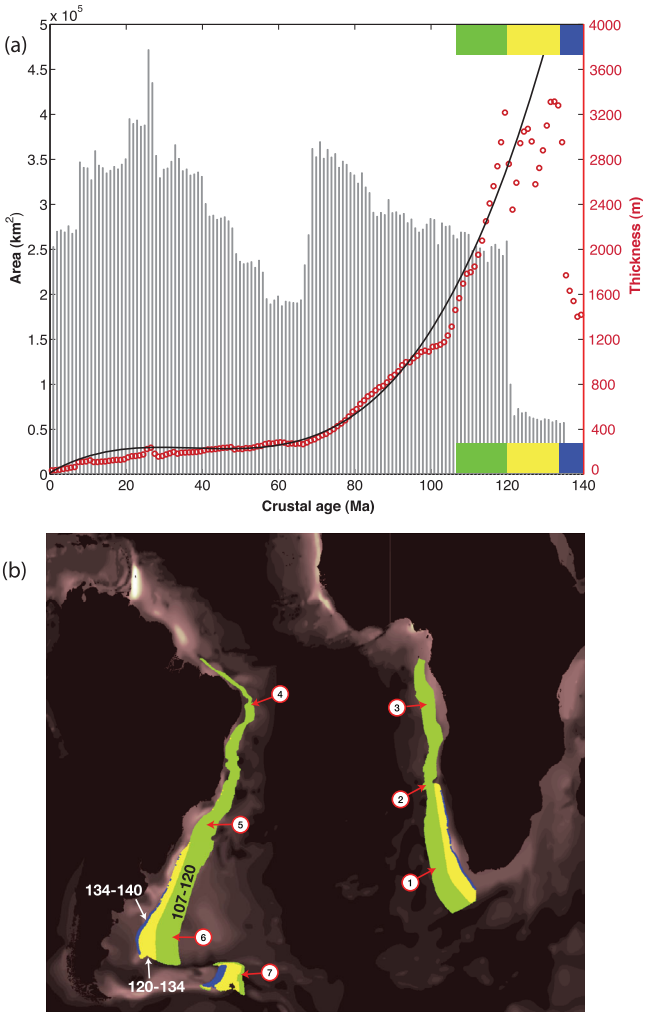

Figure 12. (a) South Atlantic Ocean sediment thickness and area versus crustal age in 1 Ma bins. Dots indicate sediment thickness bin means, bars indicate crustal area in each age bin. Coefficients of the cubic polynomial fit are given in Table 2. Color bars indicate crustal age bands. (b) Map of South Atlantic sediment thickness showing crustal age bands in Ma and basin structures that accommodate the sediment spike: 1 = Cape Abyssal Plain; 2 = Walvis Ridge; 3 = Angola Plain; 4 = Eastern Pernabuco Plain; 5 = Santos Plateau; 6 = West of Argentine Plain; 7 = East of Falkland Plateau.

global profile, cubic polynomials best fit all of the basin profiles, although the Indian Ocean profile hardly differs from linear, and there is little difference between quadratic and cubic fits in the South Atlantic.

None of the profiles in Figure 10 offer tangible evidence as to the origin of the sediment spikes seen in the global thickness profiles in Figure 7 or Figure 8. Evidence that bears on how those spikes were produced comes from the relationship between the locations of the thick ocean sediment piles and the tectonic history of each basin, as illustrated in Figures 11–14. The top plot in each of these figures shows the profile of sediment thickness versus crustal age superimposed on the crustal area versus age distribution for each basin, with color bars indicating crustal age ranges of the sediment spikes. Cubic polynomial fits of thickness versus crustal age are also shown, with coefficients given in Table 2. The bottom maps in Figures 11–13 show the locations within the ocean basin where those ranges of crust age are found, and identifies by number the local structures that accommodate the thick sediments that form the spike in the basin profile. The names of these local structures (most are marginal structures called "basins") are listed in the figure captions.

In the North and South Atlantic, there are clear associations between the ages of the spikes in the sediment profiles and rifting events, which are identified by step increases in the crustal area versus age histograms. Figure 11 shows that sediment spikes in the North Atlantic are coincident with step increases in crustal area at 150 and 112 Ma produced by rifting events associated with the opening of the central and southern portions of the North Atlantic basin. Similarly, Figure 12 shows that the pair of sediment spikes beginning at 134 and 120 Ma in the South Atlantic profile are coincident with step increases in crustal area at those times, again associated with major rifting events that opened the South Atlantic basin.

The Indian Ocean sediment profile also has a double spike, but in this case each has a distinct origin. As shown in Figure 13, the older spike beginning at 150 Ma postdates a major rifting event that separated Africa, Antarctica, and Australia, part of the Gondwana breakup. The younger spike consists mainly of sediments deposited on the Bengal Fan. These are almost entirely of Cenozoic age, derived from erosion of the Himalayan uplift following the India-Asia collision, the sediments being deposited on 90–123 Ma ocean crust south and east of the Indian subcontinent. The widths of the spikes, measured in terms of the range of crustal ages they cover given in Table 3, do not correlate with area or spreading rate: the South Atlantic spikes cover only about 13 Myr in crustal age, whereas the North Atlantic cover 19 and 26 Myr, respectively,

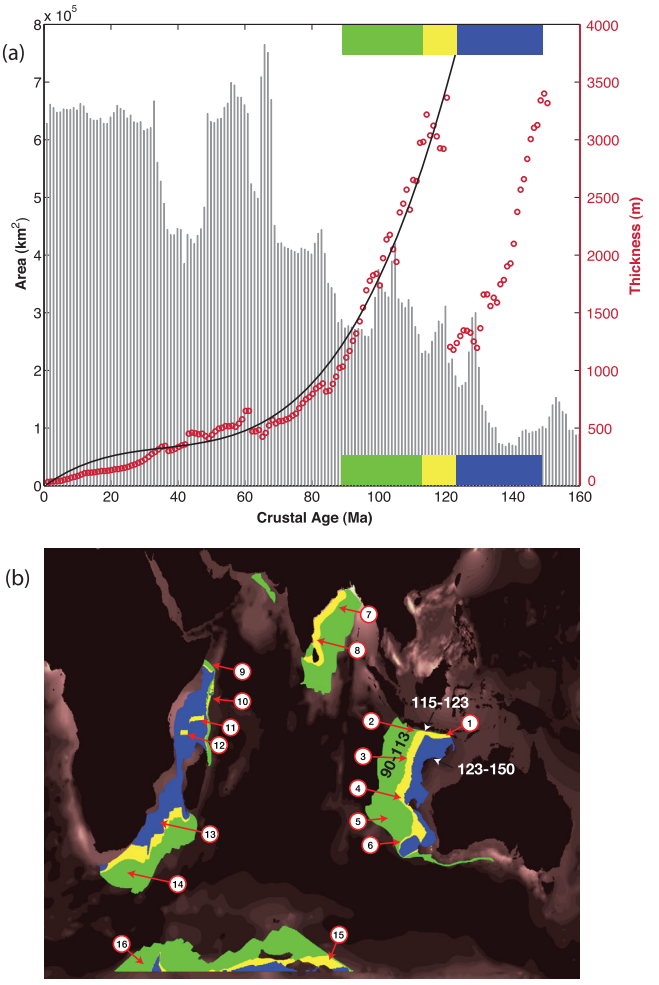

Figure 13. (a) Indian Ocean sediment thickness and area versus crustal age in 1 Ma bins. Dots indicate sediment thickness bin means, bars indicate crustal area in each age bin. Coefficients of the cubic polynomial fit are given in Table 2. Color bars indicate crustal age bands. (b) Map of Indian Ocean sediment thickness showing crustal age bands in Ma and basin structures that accommodate the sediment spike: 1 = Lombok Basin; 2 = Eastern Sunda Trough; 3 = Western Roo Rise; 4 = Southern Cuvier Plateau to Wallaby Saddle; 5 = Deep ocean north of Naturaliste Plateau; 6 = South of Dirk Hartog Ridge; 7 = Northwestern Bay of Bengal; 8 = Western Bay of Bengal; 9 = North of Somali Basin; 10 = Southern Somali Basin; 11, 12 = South of Somali Basin; 13 = Eastern Natal Valley; 14 = Transkei Basin; 15 = Davis Sea; 16 = Haakon VII Sea.

and the spikes on the fast-moving Indian plate cover 33 and 28 Myr, respectively. Nevertheless, their origins are clearly related to plate tectonic events.

As shown in the previous section, the steady state accumulation model tracks the observed global trend in ocean sediment thickness from 0 Ma to approximately 65 Ma crustal age, then underestimates the observed thickness at older ages. In order to determine if this applies to all ocean basins, we show in Figure 15 polynomial fits to the observed sediment thickness versus crustal age in each basin, compared with the sediment thickness for that basin predicted by the steady state accumulation model. All of the polynomial fits used for this comparison are given in Table 2.

The Indian Ocean is the only basin where the basin trends closely approximate the global ones; there the steady state accumulation model approximates the observed thicknesses to approximately 65 Ma crustal age, before deviating at older ages. In the North Atlantic, South Atlantic, and South Pacific basins, the observed thickness trends deviate from the global thickness trend, and in each case, the steady state accumulation model overestimates the observed thickness on young crustal ages and generally underestimates them on older crustal ages. The North Pacific basin is anomalous in this regard, in that its sediment thickness shows very little trend with crustal age, and the low-order polynomial fit in Table 2 yields a large thickness at zero crustal age. Even so, it is the only basin in which the steady state accumulation model underestimates the sediment thickness on all ages of crust.

The large deviations on young ocean crust between the observations and the steady state model in four of the five basins reflect the heterogeneity in the ocean sediment source and depositional processes. The relatively good match between the Indian Ocean and the Global distributions is partly due to the fact that the proportion of passive and active continental margins surrounding the Indian Ocean is more similar to their global proportions, compared to the Pacific or Atlantic basins, which are dominated by active and passive margins, respectively. Another factor is the high volume of Indian Ocean sediments (see Table 1), which heavily weights this basin in the global totals.

8. Residual Sediment Thickness

Nearly all of the global trends in ocean sedimentation can be assigned to steady state or nearly steady state accumulation, with a brief interval of more rapid accumulation during 0–5 Ma, plus edge effects from

Table 3. Sediment and Crustal Age Spikes by Ocean Basin

Ocean Basin	Young Spike (Ma)	Thickness (m)	Crust Spike (Ma)	Old Spike (Ma)	Thickness (m)	Crust Spike (Ma)
Indian	123–90	3350	133–121	151–123	3400	160
N. Atlantic	112–86	2200	112	149–120	1700	150
S. Atlantic	120–107	3200	121	134–121	3300	134

anomalous sediment accumulation tied to rifting at passive continental margins and major continental collision zones. This begs the question of whether an observable signal exists in this record that can be ascribed to the effects of global changes in the Earth's climate, such as Cenozoic cooling [*Caldeira*, 1992; *Zachos et al.*, 2008] or the Cretaceous greenhouse [*Berner and Kothavala*, 2001], or to biosphere changes, such as the development of pelagic calcifiers [*Arvidson et al.*, 2014]. Theoretically, major changes in the global climate are expected to have observable effects on ocean sediment accumulation. On million year time scales, increased weathering of carbonates and carbon-bearing silicates in a warming climate should be matched by an increase in oceanic carbonate sediment accumulation, and similarly, increased weathering of silicates in a warming climate is expected to produce an increase in the rate of accumulation of oceanic silica and clays. However, such effects of gradual climate change in the ocean sediment accumulation record can be obscured by changes related to evolutionary changes in the biosphere, in particular, the evolution of pelagic calcifiers, which have forced the transition from nearshore platform carbonate deposition to open ocean deposition over the past 200–250 Ma [*Wilkinson and Walker*, 1988; *Ridgwell and Zeebe*, 2005; *Arvidson et al.*, 2014].

Untangling the effects of biosphere evolution and gradual climate change in the global inventory of ocean sediments requires far more information on sediment composition, abundance, and age distribution than used in this study. Nevertheless, it is useful to search the sediment profiles we have derived for telltale signatures of these effects. Figure 16 shows the residual sediment thicknesses versus crustal age for the global ocean and for each of the five major ocean basins, obtained by subtracting the best fitting cubic polynomial fits in Table 2 from the mean thickness versus age profiles. Defined this way, the global ocean sediment thickness residual is less than ±30 m throughout the entire Cenozoic, and never exceeds ±200 m back to 120 Ma. Thickness residuals are somewhat larger in some individual ocean basins, as expected, and some of these residuals may be attributable to tectonic or climate-related events within that basin. For example, Indian Ocean residuals are negative for 30 Myr prior to 65 Ma, then positive for the next 25 Myr. It is

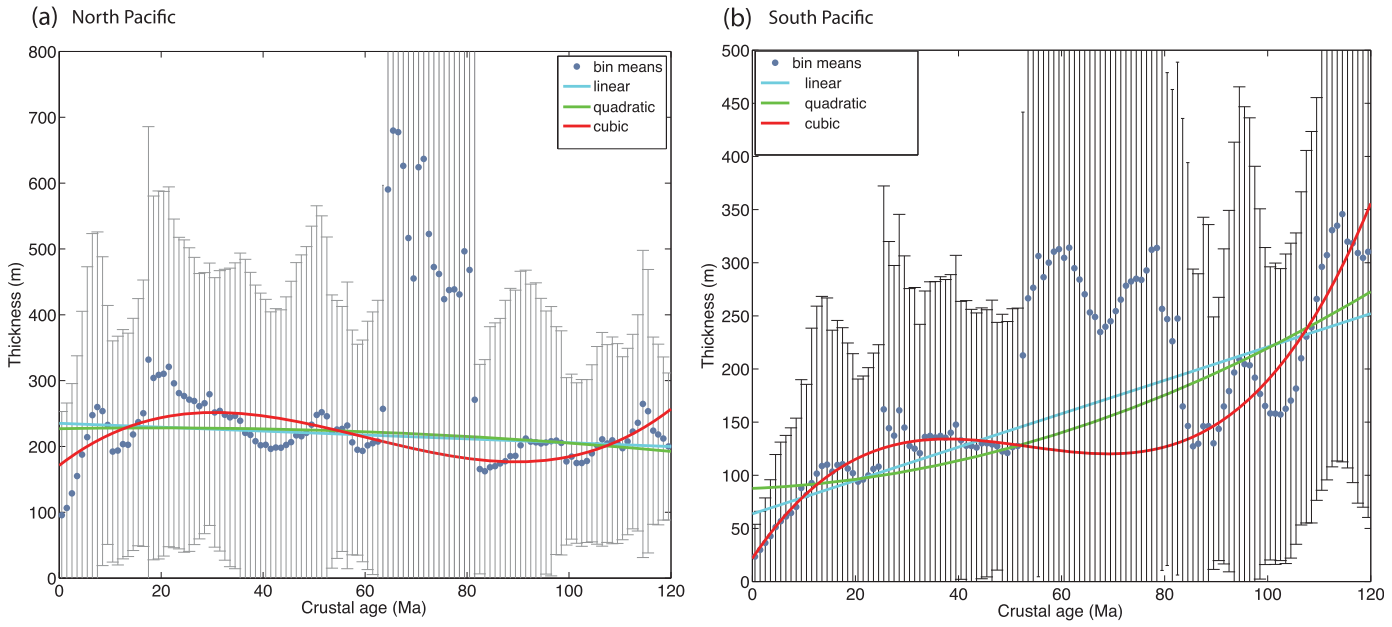

Figure 14. Pacific Ocean sediment thickness and area versus crustal age in 1 Ma bins. Dots indicate sediment thickness bin means, bars indicate crustal area in each bin. Coefficients of the cubic polynomial fit are given in Table 2. (a) North Pacific; (b) South Pacific.

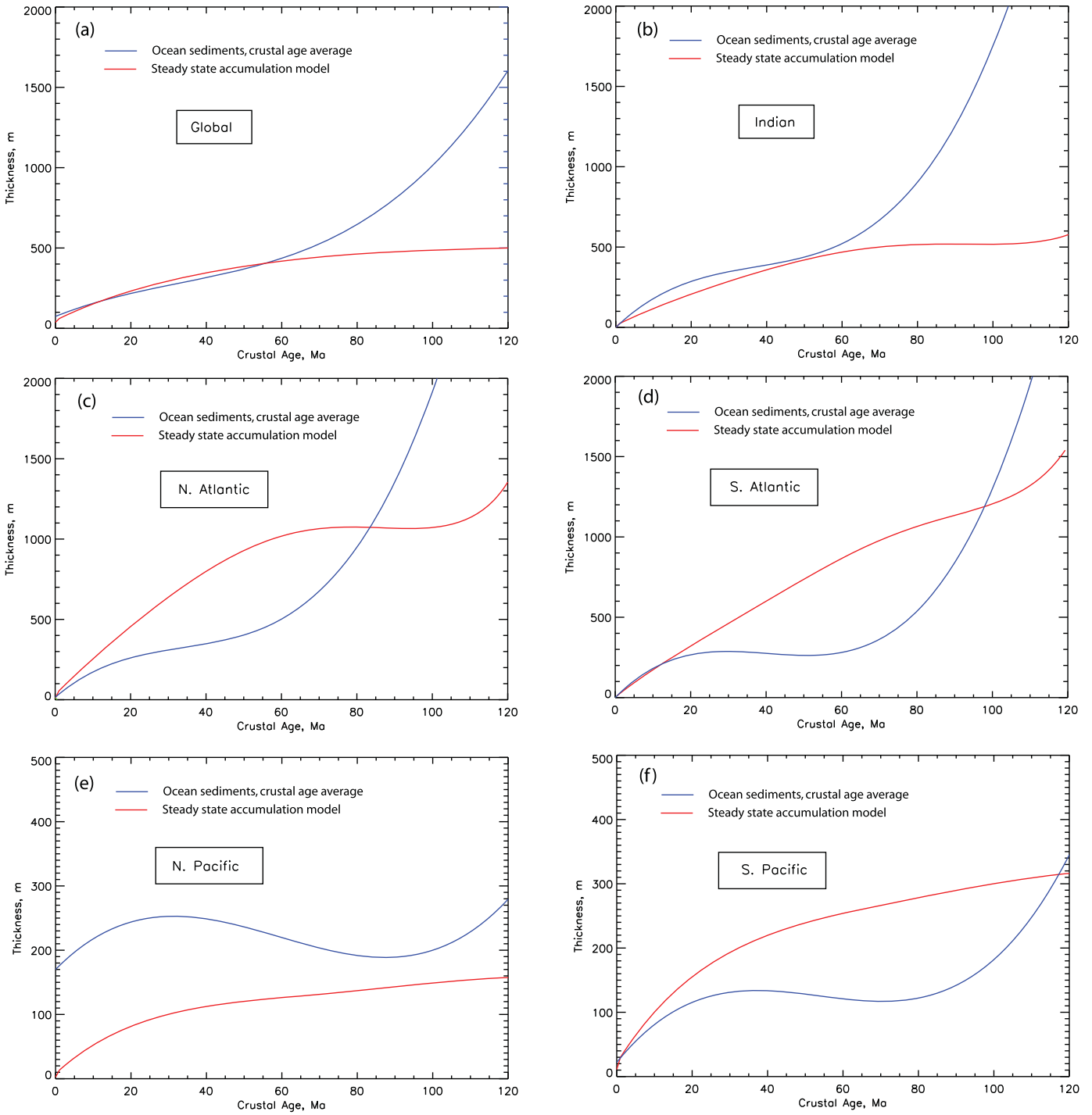

Figure 15. Observed sediment thickness versus crustal age in each ocean basin compared with the thickness predicted by the steady state accumulation model for that basin. Curves are cubic polynomial fits given in Table 2.

tempting to ascribe this behavior to increased ocean sedimentation following the emplacement of the Deccan Traps.

More significantly, perhaps, there is little coherence in the residuals between ocean basins. This lack of coherence is seen in the following correlation matrix for the sediment thickness residuals between pairs of ocean basins (NA, SA, NP, SP, and IN) and globally (G):

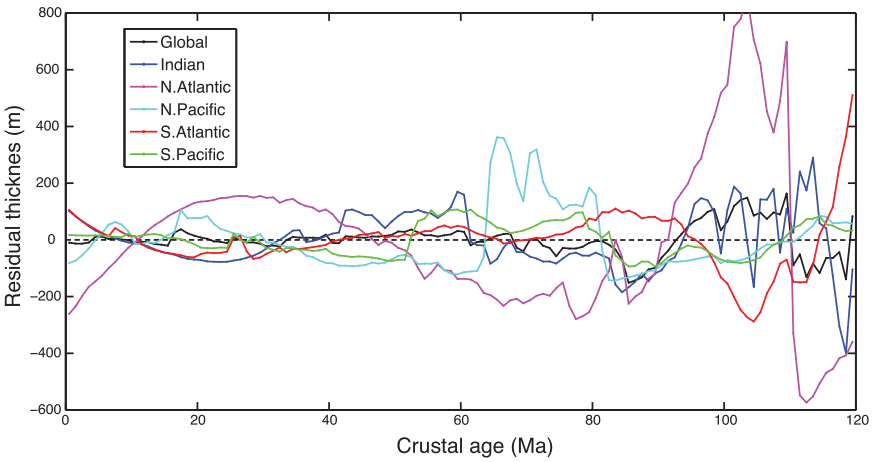

Figure 16. Residual sediment thickness by ocean basin. Mean sediment thickness minus cubic polynomial fits in Table 2 versus crustal age, for the global ocean and for each of the five ocean basins in this study.

	IN	*NA*	*NP*	*SA*	*SP*	*G*
IN	1	0.1772	−0.2656	−0.4456	0.0711	0.4444
NA	0.1772	1	−0.3079	−0.6243	−0.5772	0.7435
NP	−0.2656	−0.3079	1	0.0131	0.4131	−0.0605
SA	−0.4456	−0.6243	0.0131	1	0.2359	−0.4238
SP	0.0711	−0.5772	0.4131	0.2359	1	−0.1552
G	0.4444	0.7435	−0.0605	−0.4238	−0.1552	1

Although a few individual correlations exist, such as between the North Atlantic and the Global ocean (NA versus G), there is no overall preference for positive or negative correlations, and furthermore, the average of the nondiagonal elements is only −0.050, which indicates that the individual basin residuals are essentially uncorrelated. This argues that, once the effects of steady state accumulation and continental margins are removed, except for the anomalous 0–5 Ma accumulation, little remains in ocean sediment thickness profiles that can be attributed to other forms of global change.

9. Summary of Results

The variations of oceanic sediment thickness with crustal age have the following characteristics:

1. Ocean sediment thicknesses and modern accumulation rates show enormous scatter, but regular patterns emerge when the data are binned according to age of the underlying ocean crust. Trends in average sediment thickness and the average present-day accumulation rate are well fit by cubic polynomials in crustal age, for the global ocean and also for individual ocean basins. However, there are large differences between trends in the Atlantic and Indian Oceans versus the Pacific. In particular, the North Atlantic, South Atlantic, and Indian Oceans include sediment thickness spikes that are attributable to continental rifting and continent collision events, which are missing from the Pacific.
2. Modern ocean sediment accumulation rate patterns, extrapolated into the past assuming steady state conditions, account within uncertainties for the global average sediment thickness pattern on 0–65 Ma

(Cenozoic age) crust. The anomalously thick sediment that has accumulated on older (Mesozoic age) crust is well modeled by diffusive transport into the ocean basin from a constant flux source of sediment located on the continental margin.

3. Apart from the anomalous 0–5 Ma (Quaternary age) accumulation, we are unable to identify signatures in ocean sediment thickness that are clearly attributable global climate change. Instead, we find that the relatively small deviations from the increase in average sediment thickness with crustal age predicted by our simple accumulation model are uncorrelated across ocean basins, implying that these deviations are attributable to regional variability, rather than global climate effects.

Acknowledgments
We gratefully acknowledge support from Frontiers in Earth System Dynamics grant EAR-1135382 from the National Science Foundation. We also thank R. D. Müller for pointing out an error in the original submission. Data used in this study can be found at the following sites: Marine sediment accumulation rates [*Archer*, 1996a,b], http://geosci.uchicago.edu/archer/server.html; NOAA marine sediment thicknesses, https://www.ngdc.noaa.gov/mgg/sedthick/sedthick.html; NOAA ETOPO1 ocean bathymetry, https://www.ngdc.noaa.gov/mgg/global/global.html; Ages of the ocean crust [Müller et al., 2008b], ftp://ftp.earthbyte.org/earthbyte/agegrid/Palaeo/2008/Data/. These data interpolated to identical $0.1^\circ \times 0.1^\circ$ grids are available at http://openearthsystems.org/data/sediment/.
Conflicts of interest: The authors have no conflicts of interest to disclose regarding this research or this paper.
Author contributions: data were acquired by A.G. and analyzed by E.R. and A.G. E.R. prepared the figures and P.O. made the interpretations, analysis, and did the writing. L.H. did the editing.

References

Allen, P. A., and J. R. Allen (2013), *Basin Analysis: Principles and Application to Petroleum Play Assessment*, 3rd ed., 619 pp., Wiley-Blackwell, Chichester, U. K.
Amante, C., and B. W. Eakins (2009), ETOPO1 Arc-Minute Global Relief Model: Procedures, data sources and analysis, *NOAA Tech. Memo. NESDIS NGDC-24*, Natl. Geophys. Data Cent., NOAA, Boulder, Colo., doi:10.7289/V5C8276M.
Archer, D. E. (1996a), An atlas of the distribution of calcium carbonate in sediments of the deep sea, *Global Biogeochem. Cycles*, *10*(1), 159–174.
Archer, D. E. (1996b), A data-driven model of the global calcite lysocline, *Global Biogeochem. Cycles*, *10*(3), 511–526.
Arvidson, R. S., F. T. Mackenzie, and R. A. Berner (2014), The sensitivity of the Phanerozoic inorganic carbon system to the onset of pelatic sedimentation, *Aquat. Geochem.*, *20*, 343–362.
Berner, R. A. (2004), *The Phanerozoic Carbon Cycle: CO2 and O2*, Oxford Univ. Press, Oxford, N. Y.
Berner, R. A., and Z. Kothavala (2001), GEOCARB III: A revised model of atmospheric CO_2 over Phanerozoic time, *Am. J. Sci.*, *301*(2), 182–204.
Caldeira, K. (1992), Enhanced Cenozoic chemical weathering and the subduction of pelagic carbonate, *Nature*, *347*, 578–581.
Catubig, N. R., D. E. Archer, R. Franois, P. deMenocal, W. Howard, and E.-F. Yu (1998), Global deep-sea burial rate of calcium carbonate during the Last Glacial Maximum, *Paleoceanography*, *13*(3), 298–310.
Clift, P. D., H. Schouten, and P. Vannucchi (2009), Arc-continent collisions, sediment recycling and the maintenance of the continental crust, *Geol. Soc. Spec. Publ.*, *318*, 75–103.
Conrad, C. P. (2013), The solid Earth's influence on sea level, *Geol. Soc. Am. Bull.*, *125*(7/8), 1027–1052.
Crosby, A., D. McKenzie, and J. Sclater (2006), The relationship between depth, age and gravity in the oceans, *Geophys. J. Int.*, *166*(2), 553–573.
Cwienk, D. S. (1986), Recent and glacial age organic carbon and biogenic silica accumulation in marine sediments, Master's thesis, 237 pp., Univ. of R. I., Narragansett.
Davies, T. A., and T. R. Worsley (1981), Paleoenvironmental implications of oceanic carbonate sedimentation rates, *SEPM Spec. Publ.*, *32*, 169–179.
Divins, D. L. (2003), *Total sediment thickness of the world's oceans and marginal seas*, NOAA Natl. Geophys. Data Cent., Boulder, Colo.
Dutkiewicz, A., R. D. Müller, S. O'Callaghan, and H. Jonasson (2015), Census of seafloor sediments in the world's ocean, *Geology*, *43*, 795–798, doi:10.1130/G36883.1.
Gabet, E. J., and S. M. Mudd (2009), A theoretical model coupling chemical weathering rates with denudation rates, *Geology*, *37*, 151–154.
Goudie, A. S., and H. A. Viles (2012), Weathering and the global carbon cycle: Geomorphological perspectives, *Earth Sci. Rev.*, *113*, 59–71.
Gu, X., R. Tenzer, and V. Gladkikh (2014), Empirical models of the ocean-sediment and marine sediment-bedrock density contrasts, *Geosci. J.*, *18*, 439–447.
Hamilton, E. L. (1976), Variations of density and porosity with depth in deep-sea sediments, *J. Sediment. Petrol.*, *46*(2), 280–300.
Hay, W. W., J. L. I. Sloan, and C. N. Wold (1988), The mass/age distribution of sediments on the ocean floor and the global rate of loss of sediment, *J. Geophys. Res.*, *93*(B12), 14,933–14,940.
Howell, D. G., and R. W. Murray (1986), A budget for continental growth and denudation, *Science*, *233*, 446–449.
Lisitzin, A. P. (1996), *Ocean Sedimentation: Lithology and Geochemistry*, edited by C. Woolhiser, AGU, Washington, D. C.
Mackenzie, F. T., and J. W. Morse (1992), Sedimentary carbonates through Phanerozoic time, *Geochim. Cosmochim. Acta*, *56*, 3281–3295.
Molnar, P. (2004), Late Cenozoic increase in accumulation rates of terrestrial sediment: How might climate change have affected erosion rates?, *Annu. Rev. Earth Planet. Sci.*, *32*, 67–89.
Müller, R. D., M. Sdrolias, C. Gaina, B. Steinberger, and C. Heine (2008a), Long-term sea-level fluctuations driven by ocean basin dynamics, *Science*, *319*, 1357–1362.
Müller, R. D., M. Sdrolias, C. Gaina, and W. R. Roest (2008b), Age, spreading rates, and spreading asymmetry of the world's ocean crust, *Geochem. Geophys. Geosyst.*, *9*, Q04006, doi:10.1029/2007GC001743.
Ridgwell, A., and R. E. Zeebe (2005), The role of the global carbonate cycle in the regulation and evolution of the Earth system, Earth *Planet. Sci. Lett.*, *234*(3), 299–315.
Royer, D. L. (2014), Atmospheric CO_2 and O_2 during the phanerozoic: Tools, patterns, and impacts, in *Treatise on Geochemistry*, 6, 251–267, Elsevier B. V., Amsterdam.
Schubert, G., and A. P. S. Reymer (1985), Continental volume and freeboard through geological time, *Nature*, *316*, 336–339.
Smith, T. R., and F. P. Bretherton (1972), Stability of the conservation of mass in drainage evolution, *Water Resour. Res.*, *8*(6) 1506–1529.
Southam, J. R., and W. W. Hay (1977), Time scales and dynamic models of deep-sea sedimentation, *J. Geophys. Res.*, *82*(27), 3825–3842.
Spinelli, G. A., E. R. Giambalvo, and A. T. Fisher (2004), Sediment permeability, distribution, and influence on fluxes in oceanic basement, in *Hydrogeology of the Oceanic Lithosphere*, edited by E. E. Davis and H. Elderfield, pp. 151–188, Cambridge Univ. Press, Cambridge, U. K.
Veizer, J., and F. T. Mackenzie (2014), Evolution of sedimentary rocks, in *Treatise on Geochemistry*, vol. 9, 2nd ed., chap. 15, pp. 399–435, Elsevier, Oxford, U. K.
Walker, J. C., P. B. Hays, and J. F. Kasting (1981), A negative feedback mechanism for the long-term stabilization of Earth's surface temperature, *J. Geophys. Res.*, *86*(C10), 9776–9782.
West, A. J., A. Galy, and M. Bickle (2005), Tectonic and climatic controls on silicate weathering, *Earth Planet. Sci. Lett.*, *235*, 211–228.
Wilkinson, B. H., and J. C. Walker (1988), Phanerozoic cycling of sedimentary carbonate, *Am. J. Sci.*, *289*(4), 525–548.

Willenbring, J. K., and F. von Blanckenburg (2010), Long-term stability of global erosion rates and weathering during late-Cenozoic cooling, *Nature*, *465*, 211–214.

Willenbring, J. K., A. T. Codilean, and B. McElroy (2013), Earth is (mostly) flat: Apportionment of the flux of continental sediment over millennial time scales, *Geology*, *41*, 343–346.

Whittaker, J., A. Goncharov, S. Williams, R. D. Müller, and G. Leitchenkov (2013), Global sediment thickness dataset updated for the Australian-Antarctic Southern Ocean, *Geochem. Geophys. Geosyst.*, *14*, 3297–3305, doi:10.1002/ggge.20181.

Wold, C. N., and W. W. Hay (1990), Estimating ancient sediment fluxes, *Am. J. Sci.*, *290*, 1069–1089.

Zachos, J. C., G. R. Dickens, and R. E. Zeebe (2008), An early Cenozoic perspective on greenhouse warming and carbon-cycle dynamics, *Nature*, *451*(7176), 279–283.

Zhang, P., P. Molnar, and W. R. Downs (2001), Increased sedimentation rates and grain sizes 2-4 Myr ago due to the influence of climate change on erosion rates, *Nature*, *401*, 891–897.